Nano Research 2016, 9(1): 214–223
DOI 10.1007/s12274-016-0992-2
Research Article
ISSN 1998-0124
CN 11-5974/O4

Facile construction of carbon dots via acid catalytic hydrothermal method and their application for target imaging of cancer cells

Zhenggang Wang[1,§], Boshi Fu[1,§], Siwei Zou[1], Bo Duan[1], Chunyu Chang[1], Bai Yang[2], Xiang Zhou[1] (✉), and Lina Zhang[1] (✉)

[1] *College of Chemistry and Molecular Sciences, Wuhan University, Wuhan 430072, China*
[2] *State Key Laboratory of Supramolecular Structure and Materials, College of Chemistry, Jilin University, Changchun 130012, China*
[§] *These authors contributed equally to this work.*

Received: 24 November 2015
Revised: 18 December 2015
Accepted: 27 December 2015

KEYWORDS
hydrothermal method,
carbon dots,
carbon nanomaterials,
DNA-aptamer,
bioimaging

ABSTRACT

To solve the problem of high temperature or long reaction time in hydrothermal synthesis of carbon dots (CDs), a novel method based on the promoting carbonization by hydrochloric acid as catalysis was developed in present work. The acid catalyzed carbon dots (ACDs) were prepared facilely from tryptophan and phenylalanine at 200 ˚C for 2 h. In our findings, the acids could promote significantly the formation of the ACDs' carbon core, as a result of the accelerating of the carbonization due to the easy deoxidation. The ACDs showed an average size of 4.8 nm, and consisted of high carbon crystalline core and various surface groups. The ACDs exhibited good optical properties and pH-dependent photoluminescence (PL) intensities. Furthermore, the ACDs were safe and biocompatible. The experimental results demonstrated that such new ACDs were connected with DNA-aptamer by EDC/NHS reaction maintaining both the bright fluorescence and recognizing ability on the cancer cells, which so could be served as an effective PL sensing platform. The resultant DNA-aptamer with ACDs (DNA-ACDs) could stick to human breast cancer cells (MCF-7) specifically, and exhibited high sensitivity and selectivity, indicating the potential applications in the cancer cells targeted imaging fields.

1 Introduction

As newcomers to the field of nanomaterials & nanolights, carbon dots (CDs) have drawn tremendous attention owing to their fascinating photoluminescence (PL) properties, low toxicity, and photostability in recent years [1]. CDs are carbon nanomaterials with relatively small size, and have shown great impact in various applications such as sensing devices, photocatalysis or electrocatalysis, nanomedicine and

Address correspondence to Lina Zhang, zhangln@whu.edu.cn; Xiang Zhou, xzhou@whu.edu.cn

biomedical imaging [2–6]. For instance, the polyethylenimine (PEI) functionalized carbon dots (CD-PEI) have been utilized for gene delivery [7]. The fluorescence resonance energy transfer platform has been designed and applied in bioimaging and photodynamic therapy for cancer [8]. Thus, more fluorescent CDs systems need to be designed for researching and application requirement. CDs have been found to consist of a carbon core which is similar to nanocrystalline graphite and functional groups for surface-passivated [9]. The routes to fabricate CDs can be classified into "top-down" and "bottom-up" approaches [10]. Several top-down methods, which primarily based on cutting from a carbon source (soot and carbon graphite, etc.) [11], have been proposed to synthesize CDs. The bottom-up approaches are synthesized from molecule precursors including polymerization of monomer, dehydration, and carbonization [12]. Hydrothermal technology is a widely used and effective one-step bottom-up method. However, this method requires either high temperature or long reaction time to form carbon core and homogeneous size distribution [13–16]. The carbon core has been found related to the low toxicity of CDs [17, 18]. It is noted that the exploitation of new method with fast or moderate condition is challenging. Acid has been proved to be beneficial for the hydrolysis of cellulose, and has effect on photoluminescence of CDs [19, 20]. However, in most of the studies for CDs synthesis, the dehydration of nonvolatile acid was unavoidable, and the function of H^+ for the synthesis of carbon dots has been yet not clarified. However, the function of the H^+ promoting the CDs synthesis is important to design the synthesis method to prepare the CDs effectively. Thus, we attempted to study the effects of the H^+ medium on the fabrication of the CDs, hoping to search a novel method for facile construction of carbon dots and their potential applications.

For detecting cancer cells, the target molecules have to be modified on the surface of CDs. It has been reported that the abundant groups on the surface of CDs can be facilitated to be modified with versatile molecule and enhanced their functionality [21, 22]. Recently, DNA with CDs (DNA-CDs) serving as a platform for bioimaging and drug delivery have been realized, indicating great potential of DNA-CDs on target imaging [23]. Mucin 1 (MUC-1) is a glycoprotein, which overexpresses in the majority of human epithelial cancer cells, and has been confirmed as an important cancer biomarker in early cancers diagnosis [24]. It is not hard to imagine that the CDs with MUC-1 aptamers modified could bind to MUC-1 on cancer cells membrane specifically and recognize cancer cells. A worthwhile endeavor would be to study the reaction of the CDs with MUC-1 aptamers, and to evaluate their cancer cells targeted imaging.

In present work, a rapid one-step hydrothermal route with hydrochloric acid as catalysis to synthesize CDs from amino acids including tryptophan and phenylalanine was established to obtain crystalline carbon core via hydrothermal method. The hydrochloric acids could catalyze the synthesis of the carbon dots, because the polymerization and carbonization of the amino acids can be accelerated in the H^+ medium due to the easy deoxidation. In our findings, the synthesis time of CDs were shortened from 10 to 2 h. The acid catalyzed carbon dots were coded as ACDs. The gel permeation chromatography (GPC) was used as separation approaches to purify ACDs. The MUC-1 aptamers were coated on the surfaces of ACDs by EDC/NHS reaction, and biorecognition capability of DNA-aptamer with ACDs (DNA-ACDs) system was established. To evaluate the cells targeted imaging of DNA-ACDs system, the MUC-1 overexpressed MCF-7 cells were chosen as target cells. This synthesized pathway was facile and fast, which are important in the fact application. Moreover, the DNA-ACDs were biocompatible, so our research may provide important information for facile construction of carbon dots and biomedical targeted imaging.

2 Experimental

2.1 Materials

Ethyl-3-(3-dimethylaminopropyl) carbodiimide hydrochloride (EDC) and N-hydroxysuccinimide (NHS) were purchased from Sigma-Aldrich (Shanghai, PRC). DNA (MUC-1 aptamer): 5′-COOH-GCAGTTGATCC TTTGGATACCCTGGTAGTAAAAAGCGGAATTCC GG-3′ were supplied by Sangon Biological Engineering Technology & Co., Ltd. (Shanghai, China). Other

chemical reagents were of analytical grade supplied by Sinopharm Chemical Reagent Co., Ltd., and used without further purification. All solutions were prepared using ultrapure water from the Milli-Q system (Millipore, USA).

2.2 Fabrication of ACDs and DNA aptamer functionalized ACDs

The ACDs were synthesized through a hydrothermal method from amino acids. In a typical synthesis, 0.204 g L-tryptophan, and 0.165 g L-phenylalanine (1:1 mole ratio) were dissolved in 10 mL hydrochloric acid solution (0.1 mol·L^{-1}), and then carefully transferred into a 30 mL poly(tetrafluoroethylene) (Teflon)-lined autoclave, and subsequently heated at 200 ˚C for 2 h. The reactor was cooled down to room temperature automatically. The obtained brown ACDs aqueous solution was filtered through a 0.45-μm membrane to remove large or agglomerated particles. Subsequently, the clear solution was loaded onto an aqueous gel column packed with Sephadex G-100 for further purification [25]. The ACDs solids were obtained from freeze-drying purified ACDs aqueous solution and further vacuum-drying via a drying oven at 50 ˚C. The carbon dots that synthesized under the same condition but without acid were coded as NCDs.

To coat ACDs, the DNA-ACDs were synthesized by crosslinking reaction between the amino on the surface of ACDs and carboxyl on the terminal of DNA-aptamer in the aqueous solution. EDC (3 mg, 20 mmol) and NHS (6 mg, 75 mmol) was dispersed into 800 μL of ACDs aqueous solution (3.75 mg·mL^{-1}) and stirred for 15 min to activate ACDs. Sequentially, 100 μL DNA solution containing 10 μmol·L^{-1} nucleotides was added to the reaction system, and subsequently was vortexed at room temperature for 6 h. The obtained solution was introduced into an ultrafiltration system using an Amicon Ultra-4 centrifugal filter device with a molecule weight (M_W) cut off of 5 kDa (Millipore Corp., USA) for purification. The as-prepared products were stored at 4 ˚C for further experiment. To investigate the degree of modification of DNA-ACDs, DNA-aptamer was uncoupled from ACDs by acid-causing hydrolysis under pH = 2 for 2 h. The DNA-aptamer was collected by ultrafiltration system and quantitative analysis by nanodrop.

2.3 Characterization

The transmission electron microscopy (TEM) images were recorded by a JEM-2010 (HT) electron microscope (JEOL, Japan) with an accelerating voltage of 200 kV. The X-ray photoelectron spectroscopy (XPS) spectra were measured by an X-ray photoelectron spectrometer (ESCALAB 250Xi, Thermo Fisher Scientific, USA) using Al–K as the exciting source (1,486.6 eV). Fourier transform infrared (FT-IR) spectra were recorded from 4,000 to 400 cm^{-1} on a FT-IR spectrometer (NICOLET 5700, Thermo Fisher Scientific, USA) in KBr discs after being vacuum-dried for 24 h. Wide angle X-ray diffraction (XRD) was carried out on a XRD diffractometer (D8-Advance, Bruker, USA, Cu Kα radiation, 40 kV, 30 mA). UV–Vis spectra were measured with a UV-160A spectrophotometer (Shimadzu, Japan). The PL spectra were recorded with the help of a spectrofluorimeter (Shimadzu, Japan). The ACDs solids were dispersed in ultrapure water to obtain an aqueous solution with the concentration of 1 × 10^{-4} mg·mL^{-1}. The solution was put into a fluorometer quartz cell and tested at room temperature. The quantum yield (QY) of ACDs was calculated by the equation blow where the quinine sulfate in 0.1 M H_2SO_4 (literature quantum yield 0.54 at 360 nm) was chosen as a standard

$$\varphi_x = \varphi_{st} \cdot \frac{K_x}{K_{st}} \cdot \left(\frac{\eta_{st}}{\eta_x}\right)^2 \quad (1)$$

Where φ is the QY, K is the slope determined by the ratio of linear fitting curves of PL emission area to UV–Vis absorbance (λ = 360 nm). η is the refractive index. The subscript "x" refers to unknown solution and "st" to the standard. For these aqueous solutions, the η_{st}/η_x values were approximate to 1. The solutions with five different concentrations were prepared, and all of the absorption was kept below 0.1 at 360 nm excitation. The fluorescent images were measured on the UltraView VOX confocal system (PerkinElmer, USA), which attached to an inverted microscope (Nikon, Japan) with 408 nm laser excitation.

2.4 Cellular assay

ACDs were sterilized under UV for 30 min. Mouse

Raw cells (5×10^3 cells/200 μL) were incubated for 24 h. The ACDs solution with different concentration of 1, 2.5, 5, 10, 20, 50, 100 μg·mL^{-1} dissolved in PBS was added into cell, respectively, and then cultured for another 24 h. After that, 10 μL (5 mg·mL^{-1}) of MTT was added into every cell, and further incubating for 4 h. Then, the culture medium was replaced with 200 μL DMSO followed with gentle shake. The number of viable cells was evaluated by the ratio between mean absorbance (λ = 492 nm) of sample to control, and expressed as percentage viability.

In a typical experiment, about 2×10^5 mL^{-1} Raw cells were cultured in confocal dish for 24 h. Then, the cells were washed by PBS for 3 times, and added with 1 mL PBS as well as 100 μg·mL^{-1} ACDs. Subsequently, the cells were incubated at 37 ℃ for 4 h, and washed with PBS (phosphate buffer saline) for 3 times. 1 mL paraformaldehyde was added to immobilize for 10 min, followed by PBS washing for 3 times. The resultant cells were added with 1 mL PBS and observed via a confocal fluorescent microscope. The Raw cells were used in ACDs cellular imaging, and MCF-7 (human breast cancer cell line) was used for recognition of cancer cells along with HepG2 cells (human hepatocellular liver carcinoma cell line) as control. Furthermore, the cells were incubated at 4 ℃ for 1 h after the introduction of ACDs in cancer cells recognition test.

3 Results and discussion

3.1 Morphology and structure of ACDs

The morphology of ACDs was analyzed by TEM as shown in Fig. 1. The results indicated that the semi-spherical ACDs nanoparticles with an average diameter about 4.8 nm were monodispersed. The representative image of high-resolution TEM (HRTEM) revealed the high crystalline core of ACDs with the lattice spacing distances of 0.21 and 0.32 nm, which were consistent with that of in-plane lattice (100 facet) and between graphene layers (002 facet) of graphene, respectively. Interestingly, the ACDs which were synthesized under neutral solution (NCDs), exhibited smaller carbon particles with an average diameter of 1.9 nm (Fig. S1 in the Electronic Supplementary Material (ESM)). Furthermore, the NCDs showed no obvious lattice structure, indicating that the acid could promote significantly the carbonization process in the synthesis of ACDs. As well known, with acid as catalysts, the amino acids can decarboxylate into amines and easily react with amino acids [26]. Therefore, the tryptophan and phenylalanine could form dimer or oligomer, which could be separated from GPC [25]. The tryptophan-phenylalanine dimer could easily react with amino acid, which thus triggered and accelerated the polymerization process in the formation of ACDs in the acid medium. As mentioned above, the TEM results suggested that the acid promoted the dehydration and carbonization of ACDs. Therefore, the acids effectively catalyzed the synthesis of ACDs during both polymerization and carbonization process.

The elemental and groups composition of ACDs were explored by XPS, FT-IR, and XRD. The XPS spectra of ACDs are shown in Fig. 2. The result indicated that the ACDs mainly consisted of carbon, nitrogen, and oxygen. C1s spectrum (Fig. 2(b)) revealed that three different carbon atoms existed in different types. The bonding energy peaks at 284.7, 285.4, and 288.6 eV were assigned to C–C (sp^2), C–O

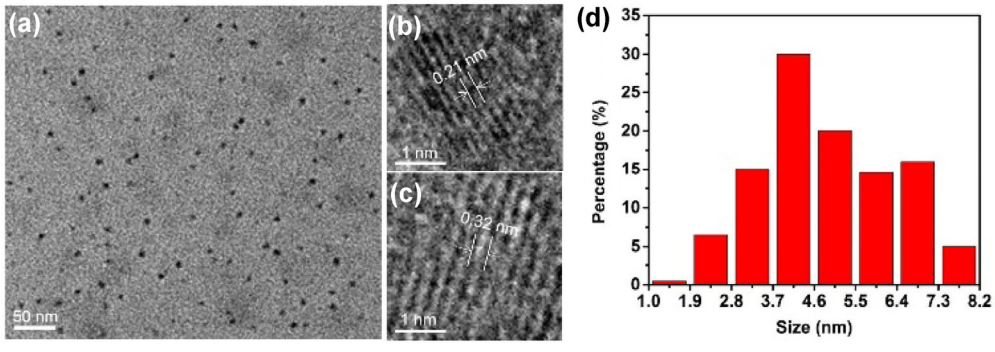

Figure 1 TEM image (a), the HRTEM images ((b)–(c)), and size distribution of ACDs (d).

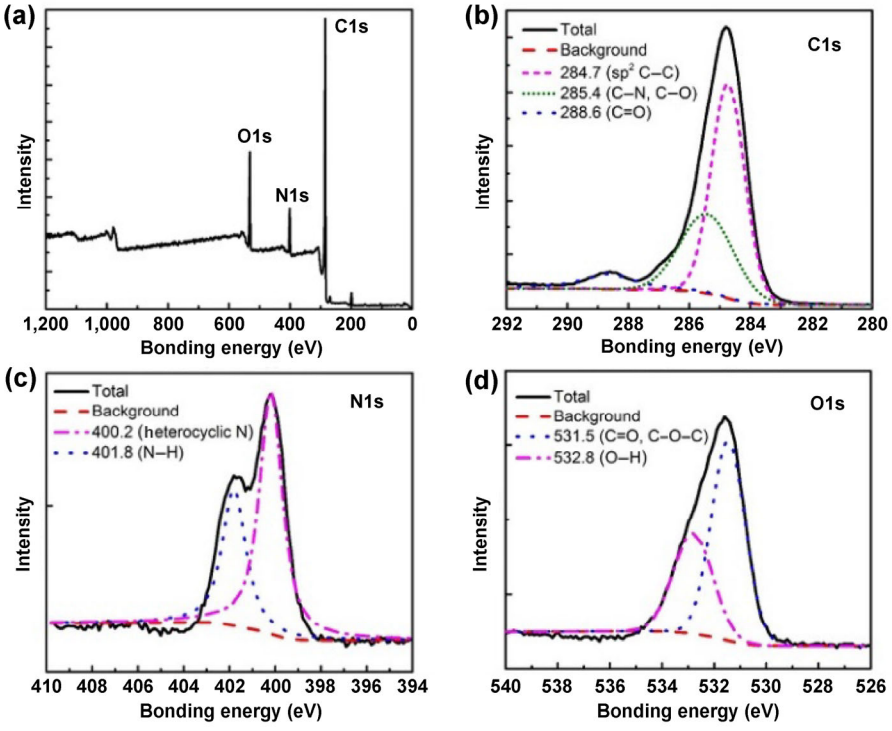

Figure 2 XPS spectra of the ACDs (a), and high-resolution of C1s (b), N1s (c), and O1s (d) peaks of ACDs.

or C–N, and C=O, respectively [27]. The bonding energy peak of C–C confirmed the graphitic structure of ACDs, which was consistent with the high crystalline graphitic core showed by HRTEM. N1s spectrum indicated that the presence of N–H and N atoms doped on graphitic structure, which correspond to 401.8 and 400.2 eV, respectively [28]. The O1s spectrum exhibited two peaks at 531.5 and 532.8 eV, attributed to C=O and O–H groups, respectively [29]. Figure 3 shows the FT-IR spectra of ACDs, as well as starting materials, tryptophan and phenylalanine. The broad absorption peaks centered at 3,500 cm^{-1} were assigned to the stretching vibrations of O–H and N–H, suggesting the formation of –OH during the synthesis of ACDs. The peak of –COOH around 3,030 cm^{-1} declined compared to tryptophan and phenylalanine, as a result of the polymerization and formation of C=ONR. The stretching modes of polycyclic aromatic C–H was observed around 2,935 cm^{-1}, and the band at 1,627 cm^{-1} was due to the absorption of C=C. The noticeable increase of C=C absorption suggested the existence of polycyclic aromatic graphite structure. The XRD pattern (Fig. S2 in the ESM) of ACDs exhibited a broad diffraction peak at $2\theta = 20°$,

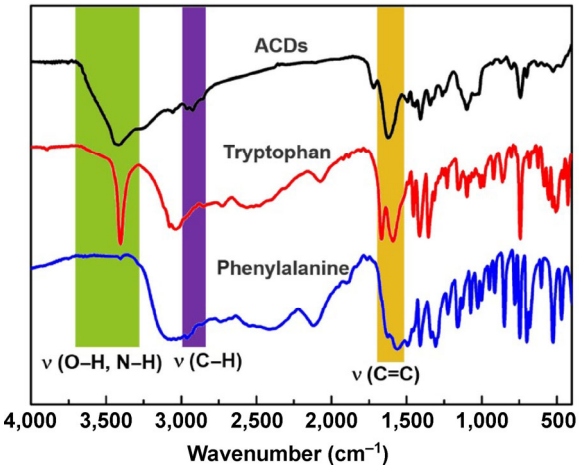

Figure 3 FT-IR spectra of ACDs, tryptophan, and phenylalanine.

attributed to the amorphous carbon. These results verified that the ACDs consist of high crystalline carbon core, amorphous carbon layer and functional groups, and there were the $–NH_2$, –OH, and –COOH groups on the surface.

3.2 Optical properties of ACDs

CDs possess bright fluorescent emissions due to the intricate origins associated with their surface defects

[30]. The optical properties of ACDs were investigated with UV–Vis spectrum and PL spectra (Fig. 4). As shown in UV–Vis spectrum, the ACDs exhibited strong absorption at 215 and 340 nm, which corresponded to π–π* transition of the aromatic C=C structure and the recombination to the surface states, respectively [4]. The ACDs displayed excellent water solubility. The transparent aqueous of ACDs could emit bright blue fluorescence, which centered at 435 nm, under 365 nm UV lamp (Figs. 4(a) and 4(b)). The quantum yield of ACDs with the excitation of 360 nm were 21%, which slightly increased, compared to NCDs (18%). Furthermore, the PL spectra illustrated that there were no obvious change for the maximum emission wavelengths of ACDs with excitation wavelength increased from 320 to 380 nm. Similarly, the ACDs exhibited clear fixed up-conversion PL around 435 nm with excitation from 660 to 760 nm (Fig. S3 in the ESM). The excitation-independent PL properties may suggest the existence of abundant groups, and high passivation degree of surface traps of ACDs [31]. Notably, the broad excitation of ACDs can provide a wide application on imaging fields, such as multiphoton bioimaging [32]. Interestingly, the PL of ACDs exhibited dependence with the pH of the solution. As shown in Fig. 5, the PL intensity reached maximum in the solution of pH 3 to 6, and it decreased in acid and especially in strong base. The stable PL emission at pH 3 to 6 was beneficial for bioimaging application. The TEM images of ACDs in pH = 1 and 13 aqueous

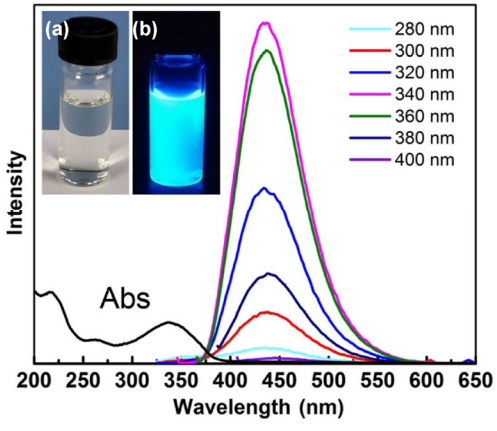

Figure 4 UV–Vis absorption and PL emission spectra of ACDs. Excitation wavelengths start from 280 to 400 nm with a 20 nm increment. Inset: photographs of ACDs aqueous solution under sun light (a) and 365 nm UV light (b).

solution were recorded (Fig. S4 in the ESM). The results demonstrated that the ACDs were easily aggregated in high pH solution. It could be explained by that the abundant $-NH_2$ on the surface of ACDs induced positive charge in H^+ rich solution to avoid ACDs aggregation, as a result of the electrostatic repulsion. However, the surface of ACDs converted to electrically neutral when pH = 13, thus led to aggregation.

3.3 Evaluation of ACDs for target imaging of cancer cells

The potential of ACDs in biological application was investigated. The toxicity impacts of the ACDs were tested by the MTT assay with Raw cells as shown in Fig. S5 in the ESM. The viability of Raw cells exhibited no significant change within the concentration of 100 $\mu g \cdot mL^{-1}$ for PL imaging. The result demonstrated the low toxicity of ACDs, which was suitable for cell imaging. It was noted that the viability of the cells cultured with NCDs showed obviously decrease. This could be explained that the crystalline carbon core contributed as a substrate, which fixed the fluorescent groups and prevented their influences on the cells. To confirm the feasibility of ACDs in cell imaging, the intracellular calibration experiment was carried out with Raw cells (Fig. S6 in the ESM). The Raw cells incubated with ACDs for 4 h at room temperature displayed relative intense blue fluorescence in cytoplasm under excitation. The result indicated the ACDs could be intake by cells, and proved a high resolution of cells imaging.

Owing to the amino groups on the surface of ACDs, the ACDs were modified conveniently, resulting in the formation of the ACDS-probe of MCF-7 cells based on aptamer–cell interaction. As shown in Fig. 6(a), the MUC-1 aptamer, which can stick to specific proteins-MUC-1, was connected to the ACDs by EDC/NHS reaction. Figure 6(b) shows the UV–Vis absorption of ACDs and DNA-ACDs. The peak at 260 nm, which was the standard absorption of DNA, increased, and no obvious change for the ACDs absorption at 340 nm was observed. The results revealed that the DNA-aptamer was coated on the surface of ACDs successfully. Zeta potential of ACDs and DNA-ACDs were recorded at pH 7.0. The zeta potential of ACDs decreased from

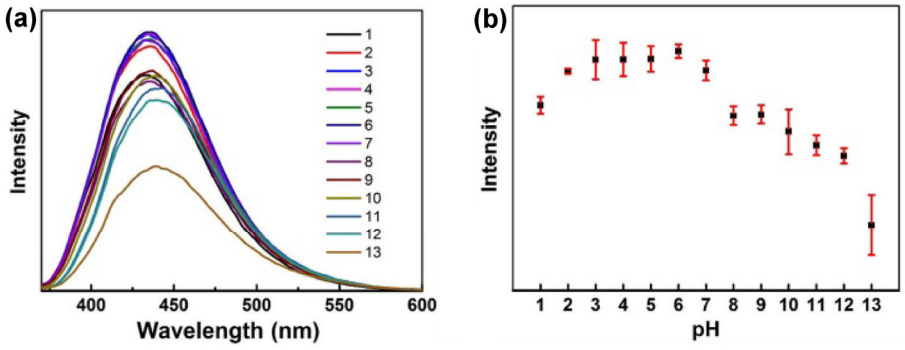

Figure 5 pH-dependent PL emission spectra of ACDs excited at 360 nm UV (a), and relative intensity variation of PL spectra with the increase of pH value from 1 to 13 (b).

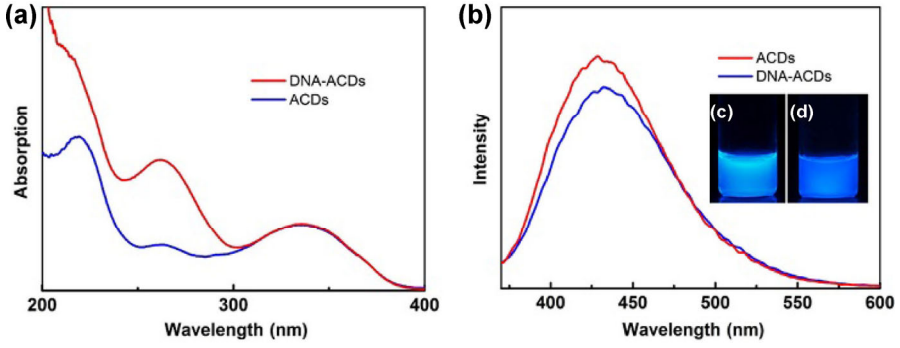

Figure 6 UV–Vis absorption (a) and PL emission spectra (b) of ACDs and DNA-ACDs. Inset: photographs of ACDs (c) and DNA-ACDs (d) aqueous solution under 365 nm UV light.

+9.0 to −15.4 mV after reacted with DNA. The positive charge of ACDs indicated that the $-NH_2$ was dominated on the surface ACDs, this was consistent with the pH-dependent PL. The $-NH_2$ was coated by negative charged DNA, leading to the negative zeta potential. The result further confirmed the formation of the DNA-ACDs composite. Moreover, the degree of modification of ACDs was analyzed to be 5.3 pmol·mg^{-1}. It was worth noting that there was no obvious change for the PL intensity of DNA-ACDs, compared to ACDs (Fig. 6(b)), indicating that the DNA modification hardly changed the optical properties of ACDs.

The biological function of as-prepared DNA-ACDs was further evaluated in target recognition of MCF-7 cells. MUC-1 protein was highly expressed in MCF-7 cells, which used to be considered as characteristic of breast cancer. The DNA-ACDs could adhere to MCF-7 cells because of the interaction of aptamer–cell, spontaneity. Figure 7 shows the fluorescent images of MCF-7 cells after cultured with DNA-ACDs. Strong blue fluorescence was observed under excitation in the DNA-ACDs, indicating the recognizing of DNA-ACDs on the MCF-7 cancer cells. However, HepG 2 cell, with low expression of MUC-1 protein, could not build the interaction with DNA-ACDs, leading to the very low fluorescence signal. The results indicated that the modification of the DNA aptamers strengthened the targeting properties of ACDs to MCF-7 cells. In view of the above results, such DNA-ACDs maintained both the PL properties of ACDs and recognizing ability of the targeting molecules on the cancer cells, which so could be served as an effective PL sensing platform. Therefore, the DNA-ACDs had potential application in cancer target imaging.

On the basis of above results, the structure of DNA-ACDs and their target imaging mechanism are proposed in Scheme 1. The acid synthesized ACDs consist of high crystalline carbon core, amorphous carbon layer and surface groups such as $-NH_2$, –OH, and –COOH, supported by data in Figs. 1–3. The $-NH_2$ on the surface of ACDs supplied the reactive site to modify DNA-aptamer. The DNA-aptamers

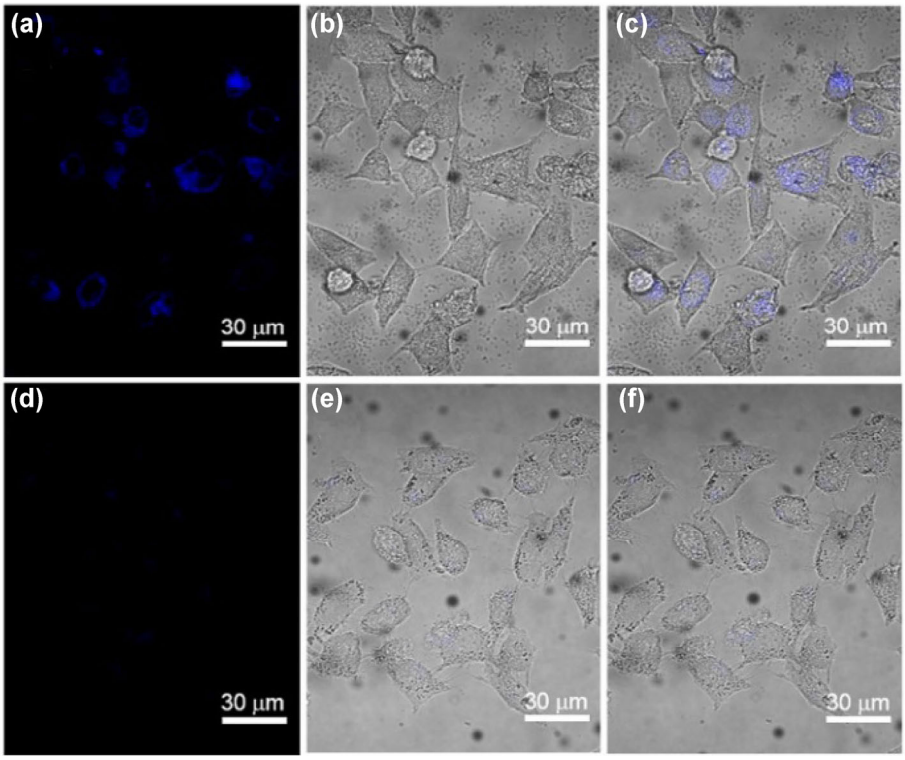

Figure 7 Confocal fluorescent images of MFC-7 cells ((a)–(c)) and HepG 2 cells ((d)–(f)) incubated with the presence of DNA-ACDs under 408 nm excitation (a) and (d), under bright filed (b) and (e), and merge images (c) and (f).

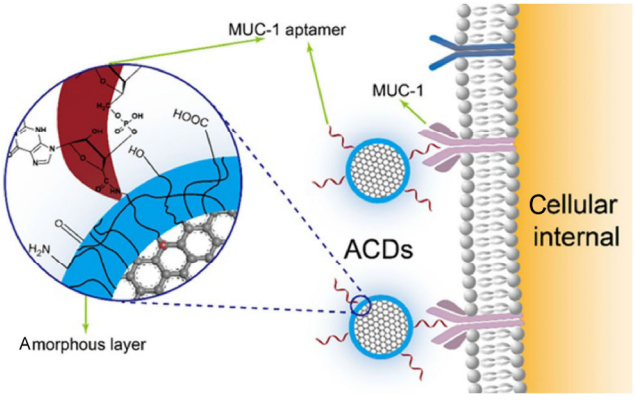

Scheme 1 Schematic diagram of architecture to DNA-ACDs and target imaging to cancer cells.

were connected with ACDs via the crosslinking reaction between the $-NH_2$ on the surface of ACDs and –COOH on the terminal of DNA-aptamers, supported by the results in Figs. 6 and 7. The fluorescent DNA-ACDs could target on cancer cells, supported by the results in Fig. 7. This could be explained by the binding interaction between DNA aptamers and MUC-1 cancer protein [33]. Therefore, the cancer cells could be detected through fluorescent imaging by using DNA-ACDs. The specific target recognition and detection were important on the diagnosis and therapies.

4 Conclusions

Biocompatible ACDs were synthesized via a hydrothermal method from tryptophan and phenylalanine with the acid as catalysis under facile and fast condition to form the high crystalline carbon core. The hydrochloric acid as catalysis played an important role for promoting the synthesis of ACDs in both the amino acids polymerization and carbonization process. The monodispersed ACDs with average diameter of 4.8 nm exhibited bright fluorescence, low toxicity and suitability for the bioimaging. The $-NH_2$ on the ACDs surface was functionalized successfully with DNA, a kind of MUC-1 aptamer, to strengthen the specificity of ACDs to MCF-7 human breast cancer cells. The as-prepared DNA-ACDs could be applied on MCF-7 cells recognition and imaging, and may serve as promising tolls in future cancer diagnosis.

Acknowledgements

This work was supported by the Major Program of National Natural Science Foundation of China (No. 21334005), the National Natural Science Foundation of China (Nos. 21304021 and 21432008), and the National Basic Research Program of China (Nos. 2010CB732203 and 2012CB720603).

Electronic Supplementary Material: Supplementary material (more TEM images, XRD pattern, up-conversion, cellular viability and cell imaging of ACDs) is available in the online version of this article at http://dx.doi.org/10.1007/s12274-016-0992-2.

References

[1] Georgakilas, V.; Perman, J. A.; Tucek, J.; Zboril, R. Broad family of carbon nanoallotropes: Classification, chemistry, and applications of fullerenes, carbon dots, nanotubes, graphene, nanodiamonds, and combined superstructures. *Chem. Rev.* **2015**, *115*, 4744–4822.

[2] Jiang, K.; Sun, S.; Zhang, L.; Lu, Y.; Wu, A. G.; Cai, C. Z.; Lin, H. W. Red, green, and blue luminescence by carbon dots: Full-color emission tuning and multicolor cellular imaging. *Angew. Chem., Int. Ed.* **2015**, *54*, 5360–5363.

[3] Zhu, A. W.; Qu, Q.; Shao, X. L.; Kong, B.; Tian, Y. Carbon-dot-based dual-emission nanohybrid produces a ratiometric fluorescent sensor for *in vivo* imaging of cellular copper ions. *Angew. Chem., Int. Ed.* **2012**, *124*, 7297–7301.

[4] Zheng, M.; Liu, S.; Li, J.; Qu, D.; Zhao, H. F.; Guan, X. G.; Hu, X. L.; Xie, Z. G.; Jing, X. B.; Sun, Z. C. Integrating oxaliplatin with highly luminescent carbon dots: An unprecedented theranostic agent for personalized medicine. *Adv. Mater.* **2014**, *26*, 3554–3560.

[5] Ge, J. C.; Jia, Q. Y.; Liu, W. M.; Guo, L.; Liu, Q. Y.; Lan, M. H.; Zhang, H. Y.; Meng, X. M.; Wang, P. F. Red-emissive carbon dots for fluorescent, photoacoustic, and thermal theranostics in living mice. *Adv. Mater.* **2015**, *27*, 4169–4177.

[6] Huang, S.; Wang, L. M.; Zhu, F. W.; Su, W.; Sheng, J. R.; Huang, C. S.; Xiao, Q. A ratiometric nanosensor based on fluorescent carbon dots for label-free and highly selective recognition of DNA. *RSC Adv.* **2015**, *5*, 44587–44597.

[7] Liu, C. J.; Zhang, P.; Zhai, X. Y.; Tian, F.; Li, W. C.; Yang, J. H.; Liu, Y.; Wang, H. B.; Wang, W.; Liu, W. G. Nano-carrier for gene delivery and bioimaging based on carbon dots with PEI-passivation enhanced fluorescence. *Biomaterials* **2012**, *33*, 3604–3613.

[8] Huang, P.; Lin, J.; Wang, X. S.; Wang, Z.; Zhang, C. L.; He, M.; Wang, K.; Chen, F.; Li, Z. M.; Shen, G. X. et al. Light-triggered theranostics based on photosensitizer-conjugated carbon dots for simultaneous enhanced-fluorescence imaging and photodynamic therapy. *Adv. Mater.* **2012**, *24*, 5104–5110.

[9] Dong, Y. Q.; Pang, H. C.; Yang, H. B.; Guo, C. X.; Shao, J. W.; Chi, Y. W.; Li, C. M.; Yu, T. Carbon-based dots co-doped with nitrogen and sulfur for high quantum yield and excitation-independent emission. *Angew. Chem., Int. Ed.* **2013**, *52*, 7800–7804.

[10] Zhu, S. J.; Song, Y. B.; Zhao, X. H.; Shao, J. R.; Zhang, J. H.; Yang, B. The photoluminescence mechanism in carbon dots (graphene quantum dots, carbon nanodots, and polymer dots): Current state and future perspective. *Nano Res.* **2015**, *8*, 355–381.

[11] Tao, H. Q.; Yang, K.; Ma, Z.; Wan, J. M.; Zhang, Y. J.; Kang, Z. H.; Liu, Z. *In vivo* NIR fluorescence imaging, biodistribution, and toxicology of photoluminescent carbon dots produced from carbon nanotubes and graphite. *Small* **2012**, *8*, 281–290.

[12] Zhu, S. J.; Meng, Q. N.; Wang, L.; Zhang, J. H.; Song, Y. B.; Jin, H.; Zhang, K.; Sun, H. C.; Wang, H. Y.; Yang, B. Highly photoluminescent carbon dots for multicolor patterning, sensors, and bioimaging. *Angew. Chem., Int. Ed.* **2013**, *52*, 3953–3957.

[13] Algarra, M.; Pérez-Martín, M.; Cifuentes-Rueda, M.; Jiménez-Jiménez, J.; Esteves da Silva, J. C. G.; Bandosz, T. J.; Rodríguez-Castellón, E.; López Navarrete, J. T.; Casado, J. Carbon dots obtained using hydrothermal treatment of formaldehyde. Cell imaging *in vitro*. *Nanoscale* **2014**, *6*, 9071–9077.

[14] Wang, C. X.; Xu, Z. Z.; Cheng, H.; Lin, H. H.; Humphrey, M. G.; Zhang, C. A hydrothermal route to water-stable luminescent carbon dots as nanosensors for pH and temperature. *Carbon* **2015**, *82*, 87–95.

[15] Pei, S. P.; Zhang, J.; Gao, M. P.; Wu, D. Q.; Yang, Y. X.; Liu, R. L. A facile hydrothermal approach towards photoluminescent carbon dots from amino acids. *J. Colloid Interf. Sci.* **2015**, *439*, 129–133.

[16] Fan, R. J.; Sun, Q.; Zhang, L.; Zhang, Y.; Lu, A. H. Photoluminescent carbon dots directly derived from polyethylene glycol and their application for cellular imaging. *Carbon* **2014**, *71*, 87–93.

[17] Yang, S. T.; Wang, X.; Wang, H. F.; Lu, F. S.; Luo, P. G.; Cao, L.; Meziani, M. J.; Liu, J. H.; Liu, Y. F.; Chen, M. et al. Carbon dots as nontoxic and high-performance fluorescence imaging agents. *J. Phys. Chem. C* **2009**, *113*, 18110–18114.

[18] Zhao, Q. L.; Zhang, Z. L.; Huang, B. H.; Peng, J.; Zhang, M.; Pang, D. W. Facile preparation of low cytotoxicity fluorescent carbon nanocrystals by electrooxidation of graphite. *Chem. Commun.* **2008**, (41), 5116–5118.

[19] Sun, B. Z.; Duan, L.; Peng, G. G.; Li, X. X.; Xu, A. H. Efficient production of glucose by microwave-assisted acid hydrolysis of cellulose hydrogel. *Bioresource Technol.* **2015**, *192*, 253–256.

[20] Wang, X. H.; Qu, K. G.; Xu, B. L.; Ren, J. S.; Qu, X. G. Microwave assisted one-step green synthesis of cell-permeable multicolor photoluminescent carbon dots without surface passivation reagents. *J. Mater. Chem.* **2011**, *21*, 2445–2450.

[21] Mazzier, D.; Favaro, M.; Agnoli, S.; Silvestrini, S.; Granozzi, G.; Maggini, M.; Moretto, A. Synthesis of luminescent 3D microstructures formed by carbon quantum dots and their self-assembly properties. *Chem. Commun.* **2014**, *50*, 6592–6595.

[22] Liu, B.; Yang, F. K.; Liu, G. Y.; Yang, X. L. Synthesis of CdS/SiO_2/polymer tri-layer fluorescent nanospheres with functional polymer shells. *Chin. J. Polym. Sci.* **2012**, *30*, 359–369.

[23] Ding, H.; Du, F. Y.; Liu, P. C.; Chen, Z. J.; Shen, J. C. DNA–carbon dots function as fluorescent vehicles for drug delivery. *ACS Appl. Mater. Inter.* **2015**, *7*, 6889–6897.

[24] Cao, H. M.; Ye, D. X.; Zhao, Q. Q.; Luo, J.; Zhang, S.; Kong, J. L. A novel aptasensor based on MUC-1 conjugated CNSs for ultrasensitive detection of tumor cells. *Analyst* **2014**, *139*, 4917–4923.

[25] Wang, X.; Cao, L.; Yang, S. T.; Lu, F. S.; Meziani, M. J.; Tian, L. L.; Sun, K. W.; Bloodgood, M. A.; Sun, Y. P. Bandgap-like strong fluorescence in functionalized carbon nanoparticles. *Angew. Chem., Int. Ed.* **2010**, *49*, 5310–5314.

[26] Jiang, J.; He, Y.; Li, S. Y.; Cui, H. Amino acids as the source for producing carbon nanodots: Microwave assisted one-step synthesis, intrinsic photoluminescence property and intense chemiluminescence enhancement. *Chem. Commun.* **2012**, *48*, 9634–9636.

[27] Sun, D.; Ban, R.; Zhang, P. H.; Wu, G. H.; Zhang, J. R.; Zhu, J. J. Hair fiber as a precursor for synthesizing of sulfur- and nitrogen-co-doped carbon dots with tunable luminescence properties. *Carbon* **2013**, *64*, 424–434.

[28] Qin, X. Y.; Lu, W. B.; Asiri, A. M.; Al-Youbi, A. O.; Sun, X. P. Green, low-cost synthesis of photoluminescent carbon dots by hydrothermal treatment of willow bark and their application as an effective photocatalyst for fabricating Au nanoparticles-reduced graphene oxide nanocomposites for glucose detection. *Catal. Sci. Technol.* **2013**, *3*, 1027–1035.

[29] Liu, S.; Tian, J. Q.; Wang, L.; Zhang, Y. W.; Qin, X. Y.; Luo, Y. L.; Asiri, A. M.; Al-Youbi, A. O.; Sun, X. P. Hydrothermal treatment of grass: A low-cost, green route to nitrogen-doped, carbon-rich, photoluminescent polymer nanodots as an effective fluorescent sensing platform for label-free detection of Cu(II) ions. *Adv. Mater.* **2012**, *24*, 2037–2041.

[30] Lim, S. Y.; Shen, W.; Gao, Z. Q. Carbon quantum dots and their applications. *Chem. Soc. Rev.* **2015**, *44*, 362–381.

[31] Li, X. M.; Zhang, S. L.; Kulinich, S. A.; Liu, Y. L.; Zeng, H. B. Engineering surface states of carbon dots to achieve controllable luminescence for solid-luminescent composites and sensitive Be^{2+} detection. *Sci. Rep.* **2014**, *4*, 4976.

[32] Cao, L.; Wang, X.; Meziani, M. J.; Lu, F. S.; Wang, H. F.; Luo, P. G.; Lin, Y.; Harruff, B. A.; Veca, L. M.; Murray, D. et al. Carbon dots for multiphoton bioimaging. *J. Am. Chem. Soc.* **2007**, *129*, 11318–11319.

[33] Ferreira, C. S. M.; Matthews, C. S.; Missailidis, S. DNA aptamers that bind to MUC1 tumour marker: Design and characterization of MUC1-binding single-stranded DNA aptamers. *Tumor Biol.* **2006**, *27*, 289–301.